

# In Situ Grignard Metalation Method for the Synthesis of Hauser Bases

Simon Sengupta<sup>+, [a]</sup>, Philipp Schüler<sup>+, [a]</sup>, Helmar Görls,<sup>[a]</sup> Phil Liebing,<sup>[a]</sup> Sven Kriek,<sup>[a]</sup> and Matthias Westerhausen<sup>\*[a]</sup>

**Abstract:** The in situ Grignard Metalation Method (*i*GMM) is a straightforward one-pot procedure to quickly produce multi-gram amounts of Hauser bases  $R_2N-MgBr$  which are valuable and vastly used metalation reagents and novel electrolytes for magnesium batteries. During addition of bromoethane to a suspension of Mg metal and secondary amine at room temperature in an ethereal solvent, a smooth reaction yields  $R_2N-MgBr$  under evolution of ethane within a few hours. A

Schlenk equilibrium is operative, interconverting the Hauser bases into their solvated homoleptic congeners  $Mg(NR_2)_2$  and  $MgBr_2$  depending on the solvent. Scope and preconditions are studied, and side reactions limiting the yield have been investigated. DOSY NMR experiments and X-ray crystal structures of characteristic examples clarify aggregation in solution and the solid state.

## Introduction

The desperate need of highly reactive yet site-selective and stereospecific metalation reagents led to the development of diverse organometallics<sup>[1]</sup> such as homometallic Grignard reagents ( $RMgX$ )<sup>[2]</sup> and Hauser bases ( $R_2N-MgX$ )<sup>[3]</sup> as well as heterobimetallic Lochmann-Schlosser bases ( $RLi/KOR'$ )<sup>[4]</sup> and inverse crowns (Mulvey reagents, for example  $M^I/M^{II}(NR_2)_3$ ) ( $M^I =$  alkali metal,  $M^{II} = Mg, Zn$ ).<sup>[5]</sup> The Lochmann-Schlosser bases and Mulvey reagents are bimetallic organometallics and represent an advancement of unimetallic mixtures of two compounds such as  $LiR/LiOR'$  or  $NaNH_2/NaR$  with different anionic bases.<sup>[6]</sup> Conversion of classical Grignard reagents and Hauser bases into heterobimetallic mixtures via addition of lithium halide alters their chemical behavior and often enhances reactivity and selectivity. Therefore, these reagents are addressed as turbo-Grignard reagents (turbo-Knochel reagents,  $RMgX/LiX$ )<sup>[7]</sup> and turbo-Hauser reagents ( $R_2N-MgX/LiX$ ).<sup>[8]</sup> Most commonly, moderately bulky diisopropylamido and 2,2,6,6-tetramethylpiperidino magnesium halides,  $(iPr_2N)MgX$  and  $(tmp)MgX$ , as well as their lithium halide adducts were applied in selective metalation reactions. However, elucidation of reaction mecha-

nisms is quite challenging because these solutions contain diverse species, which are interconnected by interfering aggregation-deaggregation equilibria and Schlenk-type ligand scrambling. Alternatively, heavy Grignard reagents such as calcium-based organometallics also exhibit significantly enhanced metalation power, occasionally leading to ether degradation side reactions.<sup>[9]</sup> Despite the fact that Hauser and coworkers<sup>[10]</sup> firstly explored synthesis and chemical behavior of amidomagnesium halides more than 70 years ago, these reagents gained tremendous interest in recent years mainly as regio- and occasionally stereoselective reagents. These Hauser bases have commonly been prepared via metalation of secondary amines with Grignard reagents. Despite extensive use of these amidomagnesium halides in inorganic, organic and organometallic chemistry, it has been recognized that the solution structures of the Hauser and turbo-Hauser bases depend on solvent and temperature as well as on the substitution pattern of the amide. Stalke and coworkers<sup>[11]</sup> employed DOSY NMR techniques to elucidate the multifaceted solution structures to identify the reactive species. Recently, we established a convenient and straightforward method to synthesize bis(trimethylsilyl)amido-magnesium halides  $(hmds)MgBr$  in a multigram scale.<sup>[12]</sup> Due to the fact that amines cannot be deprotonated by magnesium metal, Mg and bis(trimethylsilyl)amine  $H(hmds)$  are suspended in an ethereal solvent and bromoethane is added. In this in situ Grignard metalation method (*i*GMM), intermediately formed  $EtMgBr$  smoothly metalates the amine yielding  $(hmds)MgBr$  as depicted in Scheme 1 ( $R = SiMe_3$ ). This method also allowed the synthesis of carbazolyl-based Hauser and turbo-Hauser bases,  $(carb)MgBr$  and  $(carb)MgBr-LiX$  ( $X = Cl, Br$ ), and the exploitation of these heteroleptic complexes as electrolytes in magnesium batteries.<sup>[13,14]</sup>

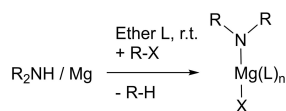
The initial promising investigations convinced us to study scope and limitations of this preparative strategy. In this study suitability of different solvents and applicability of diverse

[a] S. Sengupta,<sup>+</sup> P. Schüler,<sup>+</sup> Dr. H. Görls, Dr. P. Liebing, Dr. S. Kriek, Prof. M. Westerhausen  
Institute of Inorganic and Analytical Chemistry  
Friedrich Schiller University Jena  
Humboldtstraße 8, 07743 Jena (Germany)  
E-mail: m.we@uni-jena.de  
Homepage: www.westerhausen.uni-jena.de

[<sup>+</sup>] These authors contributed equally to this manuscript.

Supporting information for this article is available on the WWW under <https://doi.org/10.1002/chem.202201359>

© 2022 The Authors. Chemistry - A European Journal published by Wiley-VCH GmbH. This is an open access article under the terms of the Creative Commons Attribution Non-Commercial NoDerivs License, which permits use and distribution in any medium, provided the original work is properly cited, the use is non-commercial and no modifications or adaptations are made.



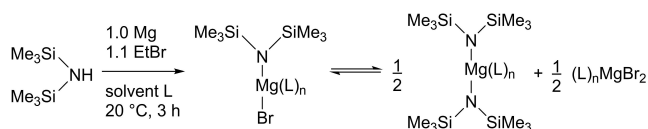
**Scheme 1.** General synthesis of amidomagnesium halides (Hauser bases) via the in situ Grignard metalation method (*i*GMM).

secondary amines for the *i*GMM were elucidated. In addition, characteristic derivatives of Hauser bases were structurally authenticated to visualize aggregation and coordination in the crystalline state.

## Results and Discussion

### Scope of the *i*GMM

In a general procedure, magnesium turnings and H(hmds) were suspended in THF and addition of bromoethane yielded nearly quantitatively heteroleptic (hmds)MgBr within three hours as depicted in Scheme 2.<sup>[12]</sup> This benchmark reaction was used to monitor the suitability of different solvents for the *i*GMM because the bis(trimethylsilyl)amides of magnesium were highly soluble in common organic solvents. In a standardized protocol, 1.0 equiv. of Mg granules and 1.0 equiv. of H(hmds) were combined in the solvent at 20 °C. Then 1.1 equiv. of bromo-



**Scheme 2.** Benchmark reaction for clarification of the suitability of organic Lewis basic solvents L for the synthesis of Hauser bases via the *i*GMM. Reaction conditions are given at the first reaction arrow. In some cases, Schlenk-type equilibria were observed, interconverting heteroleptic into homoleptic compounds (see text and Table 1).

**Table 1.** Influence of the Lewis basic solvent L on the conversion rate and on the Schlenk-type equilibrium (see Scheme 2).

Entry	Solvent L <sup>[a]</sup>	Conv./% <sup>[b]</sup>	Ratio/% <sup>[c]</sup>	$\delta(^{29}\text{Si})/\text{ppm}^{[d]}$
1	THF	92	83	−8.41/−9.46
2	2-MeTHF	92	> 95	−8.18/−
3	Et <sub>2</sub> O	94	> 95	−7.19/−
4	THP		88	−7.89/−8.67
5	MTBE	93	> 95	−7.42/−
6	Diox	71		
7	Methylal	23	87	−7.98/−8.72
8	DME	21	15	−9.14/−9.54
9	Triglyme	57	< 5	−/−9.64

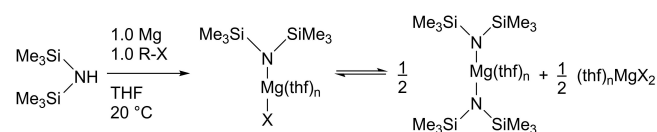
[a] Solvents: tetrahydropyran THP, methyl-tert-butyl ether MTBE, 1,3-dioxolane Diox, di(methoxy)methane Methylal, 1,2-dimethoxyethane DME, 1,2-bis(2-methoxyethoxy)ethane Triglyme. [b] Conversion of H(hmds) under the given reaction conditions. [c] Percentage of the Hauser base in the Schlenk-type equilibrium (determined by <sup>29</sup>Si NMR; ratio = [Hauser base]/sum of integrals). [d] Chemical <sup>29</sup>Si NMR shifts for (hmds)MgBr/(hmds)<sub>2</sub>.

ethane were added and after three hours an aliquot of the clear reaction mixture was hydrolyzed with 0.1 N sulfuric acid. Titration against phenolphthalein allowed calculation of the conversion rate (Table 1).

In monodentate ethers (Table 1, entries 1 to 5) a quantitative conversion of H(hmds) to the corresponding ether adducts of (hmds)MgBr was observed by <sup>29</sup>Si NMR spectroscopy. The Schlenk-type equilibrium was far on the side of the heteroleptic complexes, the real Hauser bases. 1,3-Dioxolane (entry 6) is unable to act as a bidentate Lewis base at one Mg atom, but this ether could occupy bridging positions between two magnesium centers. This property obviously reduced the conversion rate. Di(methoxy)methane (methylal, entry 7) and 1,2-dimethoxyethane (dme, entry 8) have rather small bite angles and in both cases, low conversion rates were observed. In contrast, tridentate triglyme (entry 9) led to a moderate conversion rate. In addition to the strong influence of the solvent on the conversion rate, the nature of the solvent (base strength and denticity) also affected the Schlenk-type equilibrium. It is noteworthy that the formation of the homoleptic species is favored in the oligodentate Lewis bases DME and triglyme whereas in methylal with a very small bite the formation of the heteroleptic Hauser-type complex is preferred.

The influence of the halide on the *i*GMM and on the Schlenk-type equilibrium was studied, too. For this purpose, *n*BuCl, EtBr and EtI were used to initiate the magnesiation of H(hmds) in THF at room temperature, applying an exact 1.0:1.0 molar ratio of Mg and RX (Scheme 3). Several factors are influenced by the hardness of the halide: (i) ionicity of the Mg–X bond (and hence the salt character), (ii) preferred coordination and (iii) strength of the C–X bond. In general, the Grignard-type reaction, i.e. the insertion of Mg into the C–X bond (umpolung of the carbon atom), proceeded more smoothly with increasing radius of the halogen atom. The hardness of the halide determined the preferred coordination behavior in dinuclear Hauser bases; small chloride ions occupied bridging positions as observed for for example (thf)Mg(tmp)Cl<sup>[15]</sup> and (Et<sub>2</sub>O)Mg(hmds)Cl<sup>[16]</sup> whereas the soft iodide ions favored terminal binding modes and then the amido ligands were in bridging positions (depending on the bulkiness of the amido substituents).

In Table 2, the result of this investigation is summarized. The use of chlorobutane required prolonged reaction times for satisfactory conversion rates (entry 1). The best choice was bromoethane (entry 2) which was also applied in the benchmark reaction of Scheme 2. Surprisingly, iodoethane (entry 3) did not lead to shorter reaction periods but to significantly lower conversion rates even after long reaction times.



**Scheme 3.** Influence of the alkyl halide on the *i*GMM in THF at 20 °C (see text and Table 2).

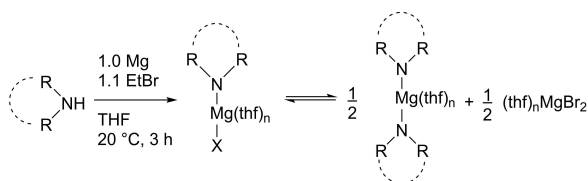
**Table 2.** Influence of the alkyl halide on the conversion rate and on the Schlenk-type equilibrium (see Scheme 3).

Entry	R-X	Conv./% (3 h) <sup>[a]</sup>	Conv./% (18 h) <sup>[b]</sup>	Ratio/ % <sup>[c]</sup>	$\delta(^{29}\text{Si})$ / ppm <sup>[d]</sup>
1	<i>n</i> Bu-Cl	2	75	77	-8.80/-9.64
2	Et-Br	78	82	83	-8.44/-9.50
3	Et-I	21	32	< 5	-/-9.53
4	Ph-Br	-	95	75	-8.44/-9.51

[a] Conversion of H(hmds) under the given reaction conditions after 3 h. [b] Conversion of H(hmds) under the given reaction conditions after 18 h. [c] Percentage of the Hauser base in the Schlenk-type equilibrium (determined by  $^{29}\text{Si}$  NMR; ratio = [Hauser base]/sum of integrals). [d]  $^{29}\text{Si}$  NMR chemical shifts for (hmds)MgX/Mg(hmds)<sub>2</sub>.

Substrate screening was performed applying the optimized conditions and using a suspension of Mg granules, secondary amine and bromoethane in THF at 20 °C as depicted in Scheme 4. After three hours the reaction mixture was quenched with sulfuric acid (aryl substituted amines) or benzoic acid (alkylamines) and the amount of formed amide was determined by titration. We focused on the conversion, i.e. consumption of the secondary amine during the *i*GMM. Representative examples were chosen, including acyclic and cyclic amines as well as alkyl and aryl substituted ones.

The conversion of the secondary amines in dependency of the substituents according to Scheme 4 is summarized in Table 3. As described above, the synthesis of (hmds)MgBr/Mg(hmds)<sub>2</sub> via the benchmark reaction (entry 1) is quantitative under these reaction conditions. In addition, substituted anilines (entries 2–4) also represent beneficial substrates for this protocol. The yields are lower for diisopropylamine (entry 5) due to a decelerated conversion rate. Cyclic amines (piperidines, entries 6–8) show an unexpected trend because increasing

**Scheme 4.** Substrate screening for the *i*GMM in THF at 20 °C (see text and Table 3).**Table 3.** Screening of the amine substrates with respect to conversion rate in the *i*GMM in THF at 20 °C and within three hours (see Scheme 4).

Entry	Substrate <sup>[a]</sup>	Conv./% <sup>[b]</sup>	Entry	Substrate <sup>[a]</sup>	Conv./% <sup>[b]</sup>
1	H(hmds)	> 99	5	HN( <i>i</i> Pr) <sub>2</sub>	65
2	HNPh <sub>2</sub>	95	6	H(pip)	0
3	HN(Me)Ph	81	7	H(dmp)	68, > 95 <sup>[c]</sup>
4	HN(C <sub>6</sub> F <sub>5</sub> ) <sub>2</sub>	96	8	H(tmp)	74, > 99 <sup>[c]</sup>

[a] Substrates: hexamethyldisilazane H(hmds), piperidine H(pip), dimethylpiperidine H(dmp), tetramethylpiperidine H(tmp). [b] Conversion of the H-acidic substrate under the given reaction conditions (see text and Scheme 4). [c] Reaction temperature: 0 °C.

methylation in 2,6-positions (and hence increasing steric hindrance) enhances the yields under the applied reaction conditions. The rate of conversion to the amide depended on the temperature for 2,6-dimethyl- and 2,2,6,6-tetramethylpiperidine formation (entries 7 and 8) and at 0 °C a complete conversion was observed whereas at room temperature side reactions interfered with the amide formation (see below). For unsubstituted piperidine (entry 6) another side reaction took place and minor amounts of piperidylethane formed.

To shed light on the factors that influence the outcome of the *i*GMM, we altered the reaction conditions for the magnesiumation of H(dmp) and H(tmp) according to the *i*GMM protocol (Scheme 4, Table 4). Lower reaction temperatures (entries 3 and 5) were advantageous whereas the concentrations played an insignificant role (entries 3 and 7). Larger excess of magnesium (entries 4 and 7) was advantageous to compensate loss due to Wurtz-type coupling reactions. The influence of the ethereal solvent THF or diethyl ether (entries 3, 7 and 9) was negligible. Performance of the *i*GMM in the presence of lithium chloride with the objective to form turbo-Hauser base reagents did not enhance the yield (entry 8).

In Table 5 the *i*GMM (Scheme 4) was monitored for cyclic unsaturated amines. The cyclic amines carbazole<sup>[14]</sup> (entry 1)

**Table 4.** Influence of reaction conditions on the conversion of 2,6-dimethyl (dmp) and 2,2,6,6-tetramethylpiperidine to the corresponding piperidine anions (see Scheme 4).

Entry	Amine	Solvent	Conc./ mol/L	Temp./ °C	Eq. Mg	Conv./ % <sup>[a]</sup>
1	H(dmp)	THF	0.5 M	r.t.	1.0	68
2	H(dmp)	THF	0.25 M	0	2.0	100
3	H(tmp)	THF	0.5 M	0	1.3	92
4	H(tmp)	THF	0.25 M	0	1.9	100
5	H(tmp)	THF	0.5 M	r.t.	1.3	74
6	H(tmp)	THF	0.25 M	r.t.	1.3	80
7	H(tmp)	THF	0.25 M	0	1.3	92
8	H(tmp) + 1 equiv. LiCl	THF	0.5 M	0	1.3	86
9	H(tmp)	Et <sub>2</sub> O	0.4 M	0	1.3	87

[a] Amide formation under the given reaction conditions after 3 h.

**Table 5.** Screening of 0.5 M THF solutions of cyclic and unsaturated amine substrates with respect to conversion rate in the *i*GMM at 20 °C until the reaction ceased (see Scheme 4).

Entry	Substrate	Conv./% <sup>[a]</sup>
1	Carbazole H(carb) <sup>[13]</sup>	96 <sup>[b]</sup>
2	Indole H(ind)	96
3	Pyrrole	58
4	2,4-Dimethylpyrrole	90
5	2,5-Dimethylpyrrole	82
6	Imidazole	22
7	Phenothiazine	88
8	Pyrazole	48
9	<i>p</i> -Tolylpyrazole	17
10	3,5-Dimethylpyrazole	82 <sup>[b]</sup>
11	3,5-Diphenylpyrazole	4
12	5-Phenyl-1 <i>H</i> -tetrazole	0
13	<i>N,N'</i> -Di(2,6-diisopropylphenyl)formamidine	44

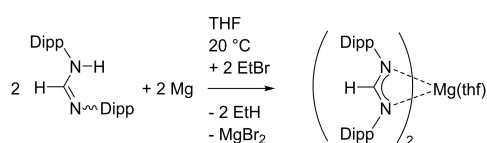
[a] Conversion of the H-acidic substrate under the given reaction conditions (see text and Scheme 4). [b] 1.5 equivalents of EtBr were added.

and indole (entry 2) as well as phenothiazine (entry 7) reacted quantitatively with Mg in THF at 20 °C within three hours after addition of bromoethane. The unsubstituted small five-membered heterocycles pyrrole (entry 3), imidazole (entry 6) and pyrazole (entry 8) showed moderate conversion under the applied conditions whereas enhanced solubility and yields were seen with methyl-substitution (entries 4, 5 and 10). In contrast to this finding, aryl substituents lowered the conversion rate (entries 9, 11 and 12) due to favored Wurtz-type coupling reactions and hence formation of butane and magnesium bromide.

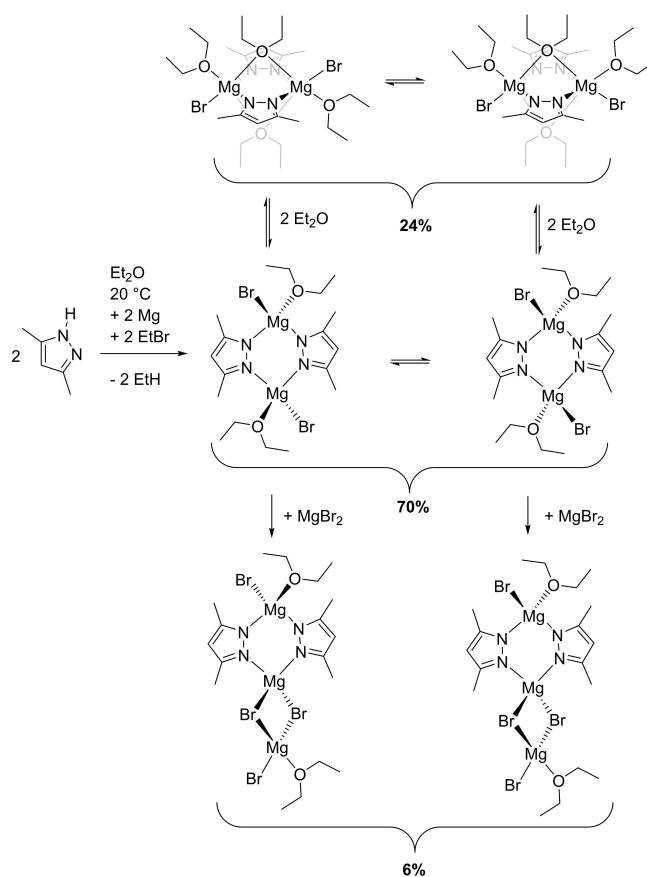
Magnesium amidinates represent an established compound class with manifold applications such as for example stabilization of very reactive magnesium complexes or reagents.<sup>[18]</sup> For this purpose, bulky *N*-bound aryl groups proved to be beneficial shielding substituents. Contrary to aryl substituted unsaturated heterocycles, acyclic *N,N'*-diarylamidines represent suitable substrates for the *i*GMM even with bulky 2,6-diisopropylphenyl (Dipp) groups (entry 13). Under standardized reaction conditions, a moderate yield of 44% for amidinate formation according to Scheme 5 was observed. This procedure led to formation of the homoleptic product as depicted in Scheme 5 and the NMR parameters were identical to published ones.<sup>[17]</sup> Again, this conversion competed with the Wurtz-type coupling reaction yielding butane and magnesium bromide and therefore, larger amounts of Mg and EtBr would be required for quantitative conversion of the amidine. Heteroleptic dinuclear *N,N'*-bis(2,6-diisopropylphenyl)formamidinato magnesium chloride with bridging chloride ligands was prepared earlier by transmetalation of an intermediately formed formamidinato bismuth dichloride compound with magnesium metal.<sup>[19]</sup>

The reaction of 3,5-dimethylpyrazole was much more complex than found for the other substrates. In the <sup>1</sup>H NMR spectrum, several species were detected. DOSY and ECC-DOSY NMR experiments verified the presence of four compounds as depicted in Scheme 6. The dinuclear 3,5-dimethylpyrazolato magnesium bromides formed transannular *cisoid* and *transoid* isomers as shown at the top of Scheme 6. Magnesium bromide (MgBr<sub>2</sub>), which formed during the Wurtz-type coupling reaction, could form an adduct with these dimers leading to unimetallic complexes as depicted in the bottom row of this scheme.

Two reasons could account for lower conversion rates. In all cases, very similar formation rates of EtMgBr could be assumed and a decelerated conversion would be caused by hindered magnesiumation of the secondary amines. Incomplete conversion could be explained by sparingly soluble magnesium amides covering the magnesium particles.

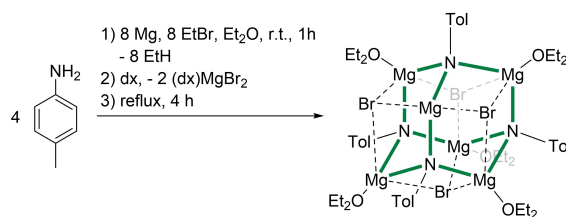


**Scheme 5.** Formation of magnesium bis[*N,N'*-bis(2,6-diisopropylphenyl)formamidinate] in tetrahydrofuran at room temperature via the *i*GMM (see text).



**Scheme 6.** Formation of [(Et<sub>2</sub>O)Mg(Pz<sup>Me2</sup>)(Br)]<sub>2</sub> in diethyl ether at room temperature via the *i*GMM and interconversion of transannular *trans*- and *cis*-isomer as well as of their magnesium bromide adducts (see text, additionally Figure S 40–42).

Primary *p*-methylaniline (*p*-tolylamine, *p*-toluidine) reacted in a similar way as the secondary amines. Thus *p*-toluidine and magnesium granules were suspended in diethyl ether and bromoethane was added within 30 minutes at room temperature. After addition of the first equivalent of EtBr, a colorless solid precipitated which redissolved during the addition of a second equivalent. After refluxing of the reaction mixture for a few hours and addition of 1,4-dioxane (dx) to precipitate magnesium bromide, the colorless magnesium imide [(Et<sub>2</sub>O)Mg]<sub>6</sub>(*N-p*Tol)<sub>4</sub>(μ<sub>3</sub>-Br)<sub>4</sub> was isolated with a yield of 59% according to Scheme 7. This structure is thermodynamically



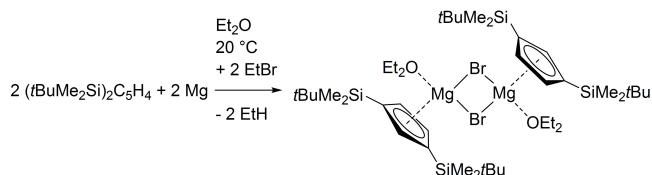
**Scheme 7.** Synthesis of the magnesium imide [(Et<sub>2</sub>O)Mg]<sub>6</sub>(*N-p*Tol)<sub>4</sub>(μ<sub>3</sub>-Br)<sub>4</sub> in diethyl ether at room temperature. The green lines clarify the Mg<sub>6</sub>N<sub>4</sub> hetero adamantane cage.

avored and it was impossible to precipitate further magnesium halide by the dioxane strategy as described earlier for Grignard reagents.<sup>[20]</sup> The central Mg<sub>6</sub>N<sub>4</sub> cage shows an adamantane-like structure, verified by an X-ray structure determination (see below), as had been observed earlier for the phenyl congener  $[(Et_2O)Mg]_6(N-Ph)_4(\mu_3-Br)_4$  which had been prepared via the classical metalation of aniline with ethylmagnesium bromide in diethyl ether.<sup>[21]</sup> In ethereal solutions, this cage compound retained its molecular structure as was verified by DOSY NMR spectroscopy.

Bulkier 2,6-diisopropylaniline (2,6-diisopropylphenylamine) can be magnesiated once in a very similar procedure in diethyl ether. However, a second deprotonation with another equivalent of ethylmagnesium reagent is impossible and excess of EtMgBr/MgEt<sub>2</sub> can be observed besides heteroleptic  $[(Et_2O)_xMg(NH-Dipp)_{2-m}Br_m]$  ( $m = 0, 1$ ; see Figures S23–S26).

Magnesocenes, i.e. substituted bis(cyclopentadienyl)magnesium complexes, are a well-established and intensely studied substance class of broad interest.<sup>[22]</sup> Most commonly, cyclopentadienes have been metalated with Mg-based organometallics; an alternative is the addition of such reagents onto fulvenes.<sup>[23]</sup> The magnesium ions are effectively shielded by two parallel cyclopentadienide ligands leading to thermodynamically and kinetically stabilized compounds. In heteroleptic (substituted) cyclopentadienylmagnesium halides the Mg atoms are accessible for substrate molecules allowing transformations at the alkaline-earth metal atom. Heteroleptic Cp'MgX ( $X = Cl, Br$ ) are far less investigated and depending on the donor strength and the bulkiness of the coligands and of the Cp' anions, mononuclear or dinuclear molecules with bridging halide ions have been isolated; examples are  $[(Me_3Si)_3C_5H_2]Mg(tmeda)Br$ ,<sup>[24]</sup>  $[Cp^*Mg(thf)(\mu-Br)]_2$  ( $Cp^* = C_5Me_4H$ ,  $Cp^*$ ),<sup>[25]</sup>  $[CpMg(Py)(\mu-Br)]_2$ ,<sup>[26]</sup> and  $[(Cp^*)Mg(Dmf)(\mu-Br)]_2$ .<sup>[27]</sup> In addition, the dinuclear chlorido complexes  $[CpMg(OEt_2)(\mu-Cl)]_2$  and  $[(Cp^*)Mg(OEt_2)(\mu-Cl)]_2$  have been reported.<sup>[28]</sup>

Therefore, we extended our elucidation of the scope of the *i*GMM also on the CH-acidic cyclopentadiene derivatives C<sub>5</sub>H<sub>6</sub> (CpH),<sup>[29]</sup> triisopropylsilylcyclopentadiene  $[(iPr_3Si)C_5H_5, TIP^5CpH]$ <sup>[29]</sup> and bulkier 1,3-bis(*tert*-butyldimethylsilyl)cyclopentadiene  $[1,3-(tBuMe_2Si)_2C_5H_4, TBDMS^2CpH]$ . Magnesium turnings and the (substituted) cyclopentadienes were suspended in diethyl ether and then bromoethane was added at room temperature. As observed for unstrained CpH and  $TIP^5CpH$ ,<sup>[29]</sup> sterically more shielded 1,3-bis(*tert*-butyldimethylsilyl)cyclopentadiene  $TBDMS^2CpH$  reacted very similar, yielding  $[(Et_2O)Mg(TBDMS^2Cp)(\mu-Br)]_2$  as depicted in Scheme 8.

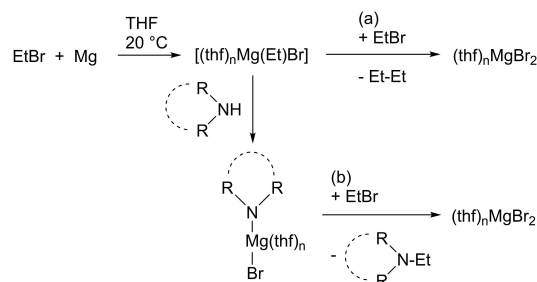


**Scheme 8.** Formation of  $[(Et_2O)Mg(TBDMS^2Cp)(\mu-Br)]_2$  in diethyl ether at room temperature via the *i*GMM (see text).

## Side reactions

There exist two possible side reactions which could interfere with the amide formation. The first step is the (rather slow) classical Grignard reaction leading to EtMgBr. This highly reactive reagent could either react with still present bromoethane to butane and magnesium bromide (Wurtz-type coupling) or with already formed magnesium amide to an ethyl amine (salt metathesis reaction) as depicted in Scheme 9. In the first case, addition of another equivalent of bromoethane and magnesium would enhance the yield, in the latter case, additional EtBr would have no impact on the final yield. A lower temperature reduces side products, and an enhanced yield was obtained (Table 3, entry 7).

For some kinetic studies the reaction solutions were kept in a sealed NMR tube to also monitor the formation of ethane. During this procedure, traces of another side product were observed during the *i*GMM, namely ethene. This small molecule H<sub>2</sub>C=CH<sub>2</sub> assumedly formed via  $\beta$ -hydride elimination from the Grignard reagent ethylmagnesium bromide. Therefore, we repeated the Grignard reaction of magnesium with bromoethane in an ethereal solution in the absence of additional *H*-acidic substrates (such as amines and cyclopentadienes) in a sealed NMR tube. Again, small amounts of ethene of up to a few percent formed verifying that  $\beta$ -hydride elimination is a common accompanying process during the formation of Grignard reagents; however, this molecule remains undiscovered in common procedures because it escapes during working in open Schlenk flasks and systems. In Figure 1, the formation of ethene is monitored for the *i*GMM of (tmp)MgBr (spectrum a) and during the preparation of the EtMgBr Grignard reagent in the absence of an amine (spectrum b). The remaining hydrido magnesium species were insoluble and hence we were unable to detect MgH functionalities by NMR spectroscopy because bulky ligands are required to produce molecular and soluble hydrido magnesium compounds.<sup>[30]</sup> In addition, it could not be excluded that the hydrido magnesium compounds acted as metalation reagents towards the amine. Obviously, this  $\beta$ -hydride elimination was an imminent process during formation of EtMgBr and could not be circumvented but a slight excess of Mg and EtBr rendered this degradation reaction harmless. We could exclude that ethene formed due to ether degradation reactions. If the *i*GMM was performed in [D<sub>8</sub>]THF, the same



**Scheme 9.** Formation of side products via Wurtz-type coupling (a) and salt metathesis reactions (b) in THF (see text).



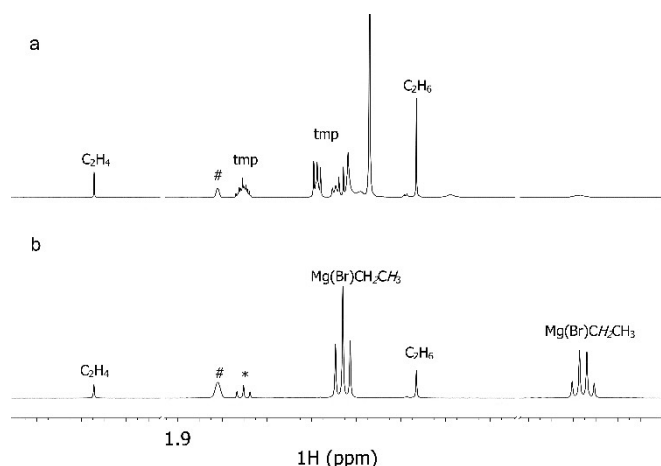


**Figure 1.**  $^1\text{H}$  NMR (400 MHz,  $[\text{D}_6]$ -THF (#), 297 K) spectroscopic detection of ethene during the *i*GMM of (tmp)MgBr in THF (a) and during the preparation of the EtMgBr Grignard reagent in THF in the absence of an amine (b) in sealed NMR tubes (chemical shifts: ethane 0.83 ppm, ethene 5.34 ppm, EtMgBr 1.16 ppm and  $-0.75$  ppm; \* residual EtBr).

amount of ethene was detected and no deuterated ethene was observed. In addition, repetition of this reaction with bromocyclohexane gave similar amounts of cyclohexene.

Ethereal ethylmagnesium bromide solutions are stable at room temperature. The  $\beta$ -hydride elimination process requires the presence of metal particles suggesting degradation of the ethyl fragment on the metal surface as depicted in Figure 2. In agreement with common mechanistic concepts,<sup>[31]</sup> the first reaction step on the metal surface is a single electron transfer from Mg onto bromoethane yielding the bromoethane radical anion. Then the bromide ion is liberated whereas the ethyl radical is trapped on the metal surface. Now the second electron transfer leads to formation of the Grignard reagent EtMgBr as the major pathway. However, a minor process may involve an electron transfer onto the  $\beta$ -hydrogen atom yielding ethene and a hydride ion as depicted in Figure 2.

A quantitative comparison of ethene evolution during a classical Grignard reaction of Mg with EtBr in THF and after addition of EtBr to a suspension of Mg granules and secondary amine in THF is depicted in Figure 3. The presence of amine slightly accelerated the ethene liberation but the amount of formed ethene is comparable for both procedures. After consumption of bromoethane the formation of ethene ceased verifying the stability of the Grignard reagent itself.

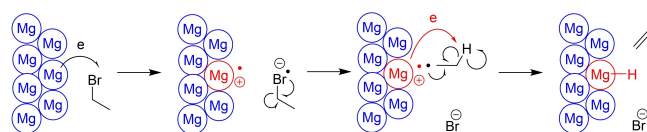


**Figure 2.** Proposed mechanism for the  $\beta$ -hydride elimination process yielding ethene.

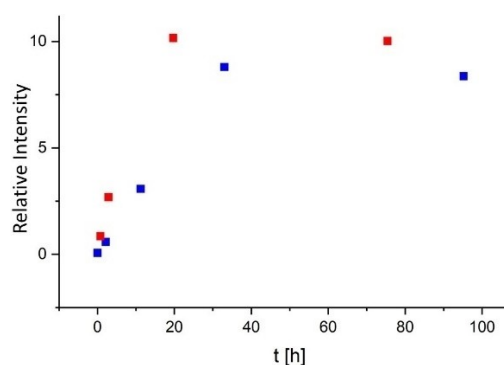


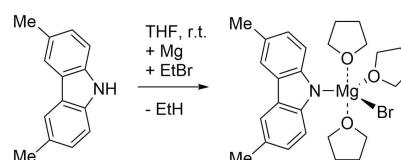
**Figure 3.** Ethene evolution during the Grignard reaction of magnesium with bromoethane (blue) and during the *i*GMM after addition of bromoethane to a suspension of Mg turnings and secondary amine in THF (red).

### NMR Spectroscopic Studies

To monitor the *i*GMM, bromoethane was added to a suspension of 3,6-dimethylcarbazole  $[\text{H}(\text{carb-3,6-Me}_2)]$  and magnesium in  $[\text{D}_6]$ THF at room temperature as depicted in Scheme 10. The methyl groups of this heterocyclic derivative allowed to monitor the proceeding reaction.

The methyl groups could be observed in the  $^1\text{H}$  NMR spectrum at approx. 2.5 ppm (Figure 4). Within several hours, the resonances of the substrate  $\text{H}(\text{carb-3,6-Me}_2)$  vanished and the intensity of the signals of the magnesium complex  $[(\text{thf})_3\text{Mg}(\text{carb-3,6-Me}_2)\text{Br}]$  increased. In this smooth and straightforward procedure, no side products were recognized. Up to a few hours the substrate bromoethane and the product ethane could be observed at the same time. This slow conversion guaranteed a smooth progression of the metalation reaction. The intermediately formed ethylmagnesium bromide was not identified in this reaction mixture because formation of the Grignard reagent was slower than its consumption.

Contrary to this reaction, the conversion of toluidine to the magnesium complex  $[(\text{Et}_2\text{O})\text{Mg}]_6(\text{N-pTol})_4\text{Br}_4$  (according to Scheme 6) clearly showed the intermediate formation of ethylmagnesium bromide as depicted in Figure 5. Even after four days, a small amount of EtMgBr Grignard reagent was still present. The reason for this behavior was the very slow magnesiation after the first deprotonation step because the second deprotonation reaction required the removal of a proton from an anionic *p*-tolylamide. In agreement with this



**Scheme 10.** Magnesiation of 3,6-dimethylcarbazole in THF at room temperature after addition of bromoethane according to the *i*GMM yielding  $[(\text{thf})_3\text{Mg}(\text{carb-3,6-Me}_2)\text{Br}]$  (see text and for the NMR spectra Figure 1).

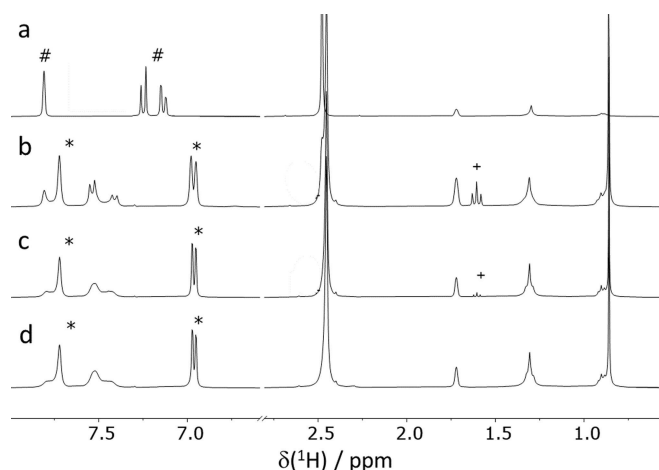


**Figure 4.**  $^1\text{H}$  NMR (400 MHz,  $[\text{D}_6]$ -THF, 297 K) spectroscopic monitoring of the *i*GMM, using 3,6-dimethylcarbazole in THF. Spectrum a shows unreacted 3,6-dimethylcarbazole (#), the bottom spectra show the proceeding reaction (b after 10 min, c after 2 h, d after 3 d; EtBr (+) and formation of 3,6-dimethylcarbazolylmagnesium bromide (\*).

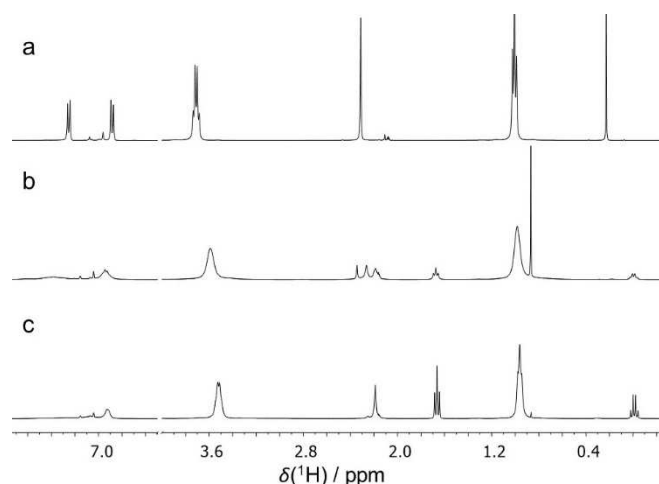


**Figure 5.**  $^1\text{H}$  NMR spectroscopic monitoring of the *i*GMM, using toluene in THF. Spectrum a shows the solution of crystalline  $[(\text{Et}_2\text{O})\text{Mg}]_6(\text{N-pTol})_4\text{Br}_4$  in  $[\text{D}_8]\text{THF}$ , at 0 ppm the resonance of  $\text{Si}(\text{SiMe}_3)_4$  is shown. Spectrum c was recorded after one hour, spectrum b after four days.

interpretation, several tolyl groups could be detected in the methyl region of the  $^1\text{H}$  NMR spectrum around 2.2 ppm.

### Molecular Structures

Slow cooling of a THF solution of  $\text{Ph}_2\text{N-MgBr}$  gave crystals of a tetragonal polymorph of the homoleptic magnesium bis(amido)  $[(\text{thf})_2\text{Mg}(\text{NPh}_2)_2]$ ; a monoclinic polymorph has been reported earlier.<sup>[32]</sup> Molecular structure and atom labelling scheme are depicted in Figure 6. The magnesium atom is in a distorted tetrahedral environment of two thf and two amido ligands. The Mg–N and Mg–O distances are equal within the estimated standard deviations. In each diphenylamido ligand the lone pair

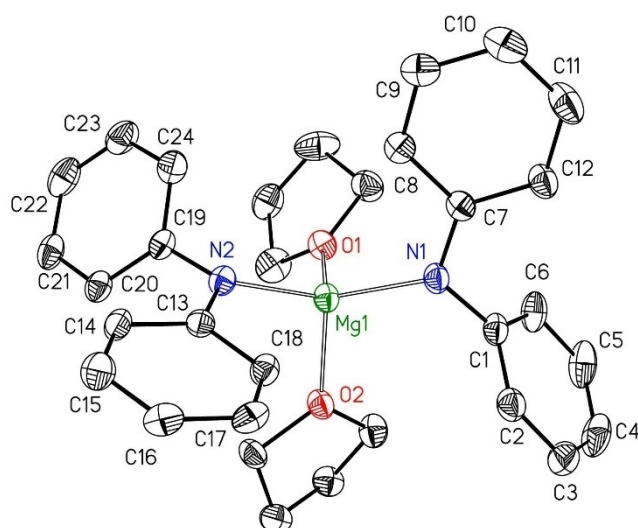


**Figure 6.** The molecular structure and atom labelling scheme of  $[(\text{thf})_2\text{Mg}(\text{NPh}_2)_2]$ . The ellipsoids represent a probability of 30%, H atoms are omitted for the sake of clarity. Selected bond lengths (pm): Mg1–N1 200.7(3), Mg1–N2 200.6(3), Mg1–O1 200.8(3), Mg1–O2 201.0(3), N1–C1 141.2(4), N1–C7 137.7(4), N2–C13 137.4(4), N2–C19 142.0(4); angles (deg.): N1–Mg1–N2 125.12(13), N1–Mg1–O1 106.68(12), N1–Mg1–O2 109.57(12), N2–Mg1–O1 109.64(13), N2–Mg1–O2 105.89(12), O1–Mg1–O2 96.12(11).

at the nitrogen atom is aligned with the  $\pi$ -system of only one phenyl group leading to a significant shortening of these N1–C7 and N2–C13 bonds by approx. 4 pm compared to the other N1–C1 and N2–C19 values. Tetra-coordination of bridging diphenylamido ligands (as in  $[\text{CpMg}\{\mu\text{-NPh}_2\}_2]$ <sup>[33]</sup> prevent such a charge backdonation into the phenyl group and hence, longer N–C bonds are observed.

Molecular structure and atom labelling scheme of heteroleptic  $[(\text{thf})_3\text{Mg}(\text{N}(\text{C}_6\text{F}_5)_2)\text{Br}]$  is depicted in Figure 7. Due to a small Mg1...F1 contact the magnesium atom is in a distorted octahedral coordination sphere, leading to an elongation of the Mg1–N1 bond by approx. 12 pm. The anionic amido and bromide ligands are cis-arranged and Br1 is in a trans-position to the Mg1...F1 contact. The back bonding of one pentafluorophenyl substituent enforces a planar arrangement of this Mg–N–C<sub>6</sub>F<sub>5</sub> moiety and a back donation of negative charge from the  $p_z(\text{N})$  lone pair into the aryl group leading to a shortened N1–C1 bond by 3 pm. The strong Mg1...F1 interaction elongates the C2–F1 bond by approx. 2 pm. Such Mg...F bonds have been observed earlier for  $[(\text{hmds})\text{Mg}(\text{N}(\text{C}_6\text{F}_5)_2)_2]$  and the homoleptic derivatives  $[(\text{thf})_2\text{Mg}(\text{N}(\text{C}_6\text{F}_5)_2)_2]$ ,  $[(\text{Et}_2\text{O})_2\text{Mg}(\text{N}(\text{C}_6\text{F}_5)_2)_2]$  and  $[\text{Mg}(\text{N}(\text{C}_6\text{F}_5)_2)_2]$ .<sup>[34]</sup>

Molecular structure and atom labelling scheme of  $[(\text{thf})_3\text{Mg}_2(\text{Pz})_2\text{Br}_2]$  are depicted in Figure 8. A very similar structure has been found for the 3,5-diphenylpyrazolate derivative  $[(\text{thf})_3\text{Mg}_2(\text{Pz}^{\text{Ph}_2})_2\text{Br}_2]$  which contains two  $\kappa^2\text{N,N}'$ -bridging pyrazolate-type ligands, two terminal thf ligands and one bridging thf molecule.<sup>[35]</sup> Homoleptic magnesium bis(pyrazolates) prefer mononuclear structures as observed for  $[(\text{tmeda})\text{Mg}(\text{Pz}^{\text{tBu}_2})_2]$ <sup>[36]</sup> and  $[(\text{HPz}^{\text{tBu}_2})_2\text{Mg}(\text{Pz}^{\text{tBu}_2})_2]$ .<sup>[37]</sup> Additional basic sites in the pyrazolyl side-arms such as 3-pyridyl-5-

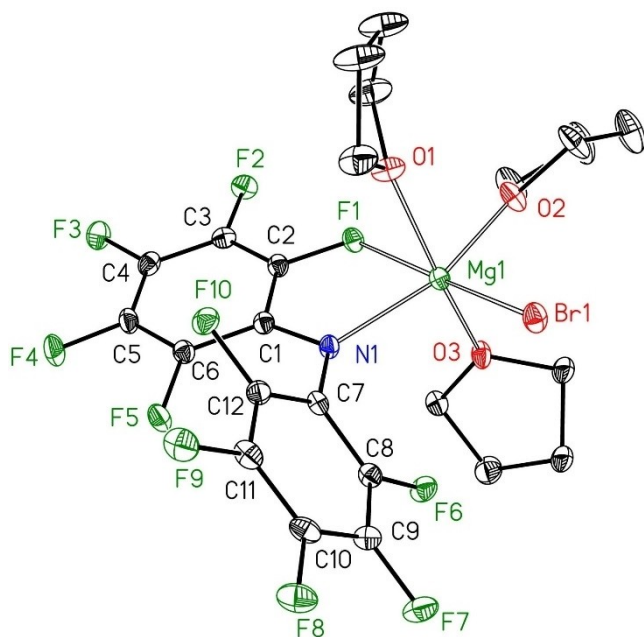


**Figure 7.** The molecular structure and atom labelling scheme of  $[(\text{thf})_3\text{Mg}\{\text{N}(\text{C}_6\text{F}_5)_2\}\text{Br}]$ . The ellipsoids represent a probability of 30%, H atoms are neglected for clarity reasons. Selected bond lengths (pm): Mg1–N1 212.89(19), Mg1–Br1 252.13(7), Mg1–O1 210.58(17), Mg1–O2 210.55(17), Mg1–O3 205.77(17), Mg1–F1 228.61(14), C2–F1 136.8(2), N1–C1 136.7(3), N1–C7 139.7(3); angles (deg.): N1–Mg1–O1 91.96(7), N1–Mg1–O2 155.23(7), N1–Mg1–O3 94.38(7), N1–Mg1–Br1 103.65(6), N1–Mg1–F1 73.91(6), O1–Mg1–O2 83.74(7), O1–Mg1–O3 160.20(8), O1–Mg1–Br1 95.69(5), O1–Mg1–F1 78.66(6), O2–Mg1–O3 82.66(7), O2–Mg1–Br1 101.05(5), O2–Mg1–F1 81.34(6), O3–Mg1–Br1 100.99(5), O3–Mg1–F1 85.11(6), Br1–Mg1–F1 173.66(5).

thienylpyrazolyl ligands can lead to stabilization of mononuclear heteroleptic pyrazolylmagnesium halides as observed for  $[(\text{thf})_3\text{Mg}(\text{Pz}^3\text{-Py-5-Th})\text{Cl}]$  ( $\text{Pz}^3\text{-Py-5-Th} = 3\text{-pyridyl-5-thienylpyrazolate}$ ).<sup>[38]</sup> The penta-coordinate magnesium atoms are in distorted trigonal bipyramidal environments with the thf bases in apical positions. The Mg1–O2 bond to the bridging ether molecule is elongated by 26 pm compared to the terminal Mg1–O1 value.

Exchange of the thf bases by bulkier and less basic diethyl ether ligands reduces the coordination number of the metal atoms. Molecular structure and atom labelling scheme of dinuclear  $[(\text{Et}_2\text{O})\text{Mg}(\text{Pz})\text{Br}]_2$  are depicted in Figure 9. The central structure is comparable to the corresponding thf adduct, but the bridging ether base is missing. Despite this change and hence related decrease of the coordination number, the Mg–N and Mg–Br bond lengths remain nearly unchanged. However, the Mg–O distance is significantly smaller than in the thf adduct where the thf bases occupy apical positions.

Molecular structure and atom labelling scheme of the magnesium imide  $[(\text{Et}_2\text{O})\text{Mg}]_6(\text{N-}p\text{ToI})_4(\mu_3\text{-Br})_4$  are depicted in Figure 10 and show the highly symmetric molecule along a  $C_2$  axis containing Mg1 and Mg1 A as well as the diethyl ether oxygen atoms O2 and O2 A. As delineated in Scheme 5, the molecule consists of an adamantane-like  $\text{Mg}_6\text{N}_4$  cage with an octahedral arrangement of the alkaline-earth metal atoms

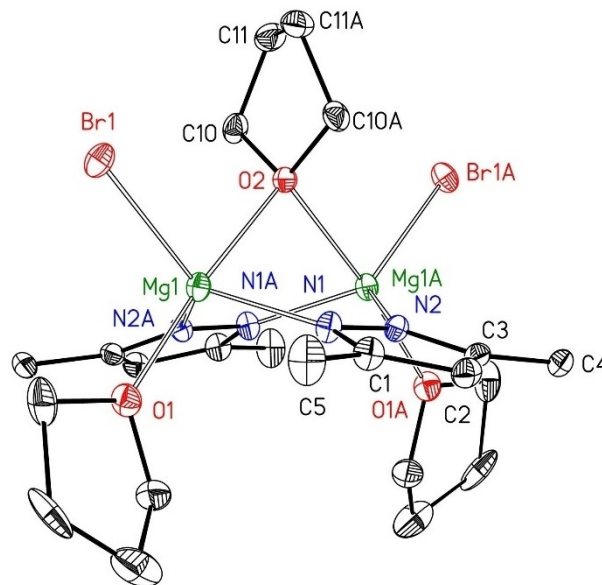


**Figure 8.** The molecular structure and atom labelling scheme of  $[(\text{thf})_2\text{Mg}_2(\text{Pz})_2\text{Br}_2]$ . The ellipsoids represent a probability of 30%, H atoms are omitted for the sake of clarity. Selected bond lengths (pm): Mg1–N1 206.1(3), Mg1–N2A 205.6(3), Mg1–Br1 247.7(11), Mg1–O1 207.9(3), Mg1–O2 233.9(2); angles (deg.): N1–Mg1–N2A 110.52(11), N1–Mg1–Br1 123.73(9), N1–Mg1–O1 94.77(12), N1–Mg1–O2 81.45(9), N2A–Mg1–Br1 123.34(9), N2A–Mg1–O1 95.00(11), N2A–Mg1–O2 81.71(9), Br1–Mg1–O1 95.62(8), Br1–Mg1–O2 90.69(7), O1–Mg1–O2 173.69(11).

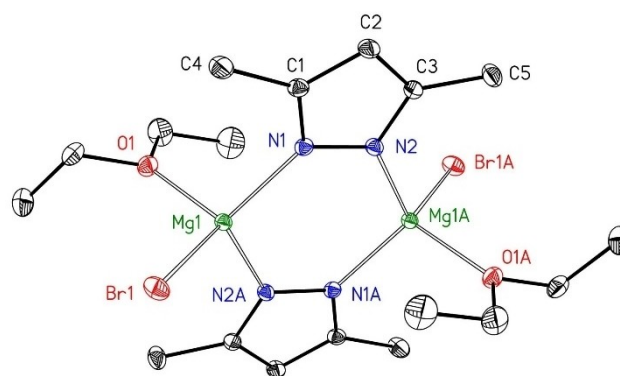


**Figure 9.** The molecular structure and atom labelling scheme of  $[(\text{Et}_2\text{O})\text{Mg}(\text{Pz})\text{Br}]_2$ . The ellipsoids represent a probability of 30%, H atoms are omitted for clarity reasons. Selected bond lengths (pm): Mg1–N1 205.74(14), Mg1–N2A 204.71(14), Mg1–Br1 247.18(6), Mg1–O1 203.60(13); angles (deg.): N1–Mg1–N2A 109.39(5), N1–Mg1–Br1 113.87(4), N1–Mg1–O1 106.67(6), N2A–Mg1–Br1 111.94(4), N2A–Mg1–O1 107.61(6), Br1–Mg1–O1 107.01(4).

(Mg...Mg distances 314.50(16) and 326.13(15) pm). Every second plane of the  $\text{Mg}_6$  octahedron is  $\mu_3$ -bridged with a nitrogen atom, the other half of the planes is capped with bromine atoms. This structure gives tetrahedral arrangements of both the bromine atoms and the nitrogen atoms. In this cage compound, the penta-coordinate magnesium atoms are in distorted trigonal bipyramidal coordination spheres with the bromine atoms in apical positions (Br1–Mg1–Br1A 170.46(6) $^\circ$  and Br1–Mg2–Br1B 170.74(4) $^\circ$ ).



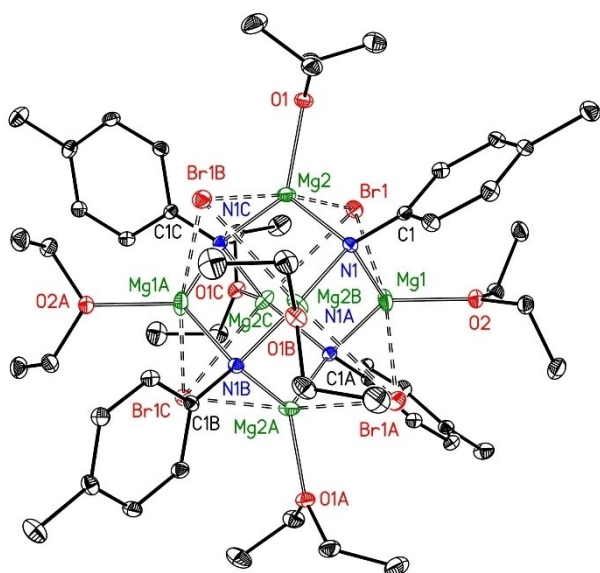


**Figure 10.** The molecular structure and atom labelling scheme of  $[(Et_2O)Mg]_6(N-pTol)_4(\mu_3-Br)_4$ . The ellipsoids represent a probability of 30%, H atoms are omitted for the sake of clarity. Selected bond lengths (pm): Mg1–N1 202.9(3), Mg1–N1A 202.9(3), Mg1–Br1 296.80(3), Mg1–Br1A 296.81(3), Mg1–O2 201.1(3), Mg2–N1 203.6(3), Mg2–N1C 204.1(3), Mg2–Br1 288.25(13), Mg2–Br1B 289.91(13), Mg2–O1 204.7(2); angles (deg.): N1–Mg1–N1A 120.20(16), N1–Mg1–Br1 90.76(7), N1–Mg1–Br1A 84.49(7), N1–Mg1–O2 119.90(8), N1A–Mg1–Br1 84.49(7), N1A–Mg1–O2 119.90(8), Br1–Mg1–Br1A 170.46(6), Br1–Mg1–O2 94.77(3), Br1A–Mg1–O2 94.77(3), N1–Mg2–N1C 117.26(13), N1–Mg2–Br1 93.07(8), N1–Mg2–Br1B 86.21(8), N1–Mg2–O1 111.46(10), N1C–Mg2–Br1 86.21(8), Br1–Mg2–Br1B 170.74(4), Br1–Mg2–O1 92.89(7), Br1B–Mg2–O1 96.07(7).

This structure is unique to the best of our knowledge and shows characteristic features. Two tolyl groups are bent toward Mg1 leading to rather short Mg1...C1 contacts of 271.7(3) pm to the *ipso*-carbon atoms. This interaction elongates the Mg1–Br1 and Mg1–Br1A bonds (296.80(3) and 296.81(3) pm) whereas the Mg2–Br1 and Mg2–Br1B distances (288.25(13) and 289.91(13) pm) are slightly smaller. The phenyl derivative  $[(Et_2O)Mg]_6(N-Ph)_4(\mu_3-Br)_4$  is much more distorted and the Mg–Br bond lengths vary in a very broad range between 276 and 348 pm.<sup>[21]</sup> Halide-free arylimido magnesium derivatives of the type  $[(thf)Mg(NAr)]_6$  (Ar = Ph,<sup>[39]</sup> 1-Naph<sup>[40]</sup>) contain hexagonal Mg<sub>6</sub>N<sub>6</sub> prisms with comparable Mg–N and Mg–O bond lengths (Table 6) which can be described as a (distorted) Mg<sub>6</sub>

**Table 6.** Comparison of selected bond lengths (pm) of the hexanuclear complexes  $[(Et_2O)Mg]_6(N-pTol)_4(\mu_3-Br)_4$  (I),  $[(Et_2O)Mg]_6(N-Ph)_4(\mu_3-Br)_4$  (II),  $[(thf)Mg(NPh)]_6$  (III), and  $[(thf)Mg(NNaph)]_6$  (IV).

	I	II	III	IV
Mg–O <sub>min</sub>	201.1(3)	199.6	199.8	201.2(5)
Mg–O <sub>max</sub>	204.7(2)	205.2	205.3	202.5(5)
Mg–Br <sub>min</sub>	288.25(13)	276.1	–	–
Mg–Br <sub>max</sub>	296.83	333.7	–	–
Mg–N <sub>min</sub>	201.1(3)	201.9	200.0	202.2(5)
Mg–N <sub>max</sub>	204.1(3)	205.5	209.4	210.5(5)
Mg...Mg <sub>min</sub>	314.50(16)	320.9	275.9	280.2
Ref.		[20]	[37]	[38]

octahedron, the nitrogen atoms cap six of the eight triangular faces.<sup>[41]</sup>

The molecular structure and atom labelling scheme of  $[(Et_2O)Mg]_6(TBDMS^2Cp)(\mu-Br)_2$  are depicted in Figure 11. The structural influence of the *tert*-butyldimethylsilyl (TBDMS) substituents on the central substructure are rather small compared to  $[(Et_2O)Mg]_6(Cp)(\mu-Br)_2$  (Mg–Br 257.8(2) and 260.9(2), Mg–O 204.4(5) pm) and  $[(Et_2O)Mg]_6(TIPSCp)(\mu-Br)_2$  (Mg–Br 258.03(7) and 261.94(8), Mg–O 206.92(16) pm).<sup>[29]</sup> In the nearly square Mg<sub>2</sub>Br<sub>2</sub> ring the Mg–Br distances are very similar, supporting rather low steric pressure induced by the bulky TBDMS<sup>2</sup>Cp anions. Furthermore, the Mg–O bond lengths to the ligated diethyl ether molecules are comparable to those of  $[(Et_2O)Mg]_6(Cp)(\mu-Br)_2$  and  $[(Et_2O)Mg]_6(TIPSCp)(\mu-Br)_2$ .

### Validation of the iGMM

Magnesium is an abundant, environmentally benign and non-toxic alkaline-earth metal and, hence, a very attractive basis for organometallics with multifaceted applications. However, low reactivity of the metal prohibits direct metalation of many *H*-acidic substrates such as amines, amidines and cyclopentadienes. Therefore, metal activation is often required to enhance the reactivity. Recent developments aim toward time-economic and resource saving procedures.

Novel protocols for the preparation of highly reactive organomagnesium reagents were developed to circumvent multiple step processes, solvent exchange during synthesis as well as time-consuming and complicated work-up procedures. Therefore, a one-pot protocol was reported for the synthesis of pyrazolates and benzamidates via intermediate phenylmagnesium iodide and 3,5-diphenylpyrazolylmagnesium iodide and magnesium bis[*N,N'*-dimesitylbenzamidate] were isolated with yields of 82% and 39%, respectively.<sup>[42]</sup> Mechanochemistry had been advanced to prepare air- and moisture-sensitive alkaline-

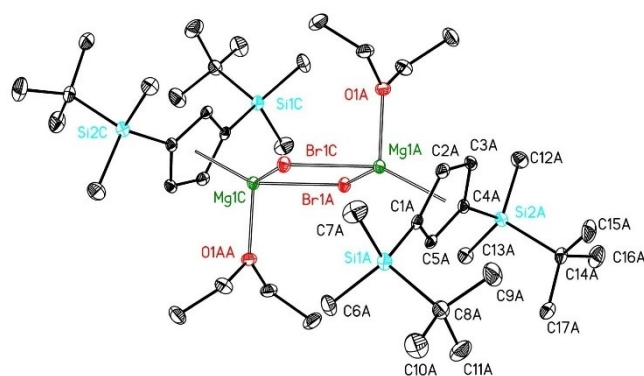


**Figure 11.** The molecular structure and atom labelling scheme of  $[(Et_2O)Mg]_6(TBDMS^2Cp)Br$ . The ellipsoids represent a probability of 30%, H atoms are omitted for the sake of clarity. Selected bond lengths (pm): Mg1A–O1A 206.4(3), Mg1A–Br1A 259.28(12), Mg1A–Br1C 261.76(13), Mg1A–C1A 243.7(3), Mg1A–C2A 243.0(4), Mg1A–C3A 243.7(3), Mg1A–C4A 243.4(4), Mg1A–C5A 239.7(3), C1A–Si1A 185.4(4), Si1A–C6A 186.9(4), SiA–C7A 187.4(4), Si1A–C8A 190.6(4), C4A–Si2A 185.1(4), Si2A–C12A 186.6(4), Si2A–C13A 186.7(4), Si2A–C14A 191.3(4).

earth metal compounds by ball milling.<sup>[43]</sup> Highly reactive organometallic potassium beryllates<sup>[44]</sup> and magnesates<sup>[45]</sup> were prepared with moderate yields as proof of concept for mechanochemical organometallic chemistry. Even though the preparation succeeded solvent-free, the product had to be extracted with an anhydrous organic solvent. Another novel device-related procedure allowed the formation of turbo-Hauser bases  $R_2NMgCl \cdot LiCl$  by running a mixture of 2-chloropropane and secondary amine in THF and toluene through a column, the front half filled with Mg metal and the back half packed with LiCl.<sup>[46]</sup> A different fascinating one-pot procedure involved a fluorous phase as liquid membrane between RI and Mg metal, covered with an organic solvent, yielding a system with three liquid phases and magnesium particles floating on the fluorous phase.<sup>[47]</sup> This setting required three liquid phases of significantly different density. RI slowly diffused through the fluorous phase and was reduced by magnesium yielding RMgI which immediately reacted with the substrate (such as ketones) dissolved in the organic top phase. This procedure was limited to iodomethane and iodoethane for density reasons and this iodoalkane phase vanished during the procedure, finally leading to a two-phase system. The *i*GMM outperforms the settings described above. The suspension of Mg granules and *H*-acidic substrate like amines smoothly reacted upon addition of inexpensive bromoethane within very few hours yielding magnesium reagents like Hauser bases. Activation of Mg prior to use was unnecessary. These solutions could be used directly for further reactions because in most cases no interfering side products formed. Side reactions such as Wurtz-type coupling reactions enhance the amount of inert magnesium bromide, and butane is volatile and very unreactive. In only very few cases, intermediately formed EtBr reacted with already formed Hauser base leading to the formation of negligible amounts of undesired  $R_2N-Et$ . Sparingly soluble Hauser base reagents could not be prepared by this *i*GMM because precipitate covered the metal particles and the reaction rather quickly ceased.

## Conclusions

The in situ Grignard Metalation method (*i*GMM), i.e. the metalation of *H*-acidic substrates with Mg granules after addition of EtBr, is a powerful tool for the synthesis of heteroleptic organylmagnesium bromides within a few hours. This smooth reaction is a straightforward strategy for large scale syntheses of heteroleptic Grignard-type compounds. The presence of acidic hydrogen atoms is a precondition for this method, but the  $pK_a$  values alone are not too meaningful. Insoluble or sparingly soluble products precipitate and cover the magnesium particles which disrupts the smooth continuation of this metalation reaction. This finding limits the choice of solvent because heteroleptic organylmagnesium halides are often significantly more soluble in ethereal solvents than in hydrocarbons.

These heteroleptic compounds show a Schlenk-type equilibrium, interconverting heteroleptic RMgBr into homoleptic

$MgR_2$  and  $MgBr_2$ . Expectedly, this ligand exchange reaction depends on the nature of the solvent (mainly base strength and bulkiness of the Lewis bases). Due to this equilibrium, cooling of the reaction mixture can favor crystallization of the homoleptic compounds as observed for  $[(thf)_2Mg(NPh_2)_2]$ .

Side reactions slightly reduce the yields which are often nearly quantitative. Wurtz-type coupling reactions of intermediately formed EtMgBr with EtBr yield magnesium bromide and volatile butane and hence, this side reaction does not produce impurities. Contrary to this side reaction, the metathetical formation of  $R-Et$  via the reaction of EtBr with already formed RMgBr causes impurities.

Execution of this *i*GMM in a sealed NMR tube shows the evolution of ethene. The observation of this molecule suggests a  $\beta$ -hydride elimination from intermediately formed EtMgBr on the surface of the alkaline-earth metal particles. This proposal has been verified by repetition of the reaction of Mg turnings with EtBr in the absence of any *H*-acidic substrate concluding that ethene formation occurs regardless of the presence of additional *H*-acidic substrates.

The bromide ion exhibits intermediate basicity and hardness. Therefore, a multifaceted coordination behavior has been observed in the solid state and in solution. Bromide ions can bind terminally as observed for the pyrazolate derivatives and can adopt  $\mu$ - (as for example in cyclopentadienide complexes) or  $\mu_3$ -bridging positions (as found in heteroleptic imides).

In summary, the *i*GMM is a powerful straightforward strategy for large-scale synthesis of many magnesium reagents. Schlenk-type equilibria may interconnect homoleptic into heteroleptic species and *vice versa*. The procedure proceeds smoothly within very few hours via the addition of EtBr to a suspension of magnesium and *H*-acidic substrate in an ethereal solvent. Preconditions include solubility of *H*-acidic substrates and organylmagnesium products RMgBr and  $MgR_2$  to safely exclude precipitation onto the Mg particles. This straightforward synthesis of magnesium reagents offers advantages such as low-priced starting materials and a time-economic process compared to other procedures.

## Experimental Section

**General information:** All manipulations were carried out under an inert nitrogen atmosphere using standard Schlenk techniques, if not otherwise noted. The solvents were dried over KOH and subsequently distilled over sodium/benzophenone under a nitrogen atmosphere prior to use. All substrates were purchased from Alfa Aesar, abcr, Sigma Aldrich or TCI and used without further purification. 3,6-Dimethylcarbazole<sup>[48]</sup> and  $HN(C_6F_5)_2$ <sup>[49]</sup> were synthesized as described in the literature. The yields given are not optimized. Purity of the compounds was verified by NMR spectroscopy. Deuterated solvents were dried over sodium, distilled, degassed, and stored under nitrogen over sodium.  $^1H$ , and  $^{13}C\{^1H\}$  NMR spectra were recorded on Bruker Avance I 250 (BBO) Bruker Avance III 400 (BBO, BBFO probes Avance neo 500 (BBFO Prodigy probe) and Avance III HD 600 (TCI cryoprobe) spectrometers. Chemical shifts are reported in parts per million relatively to  $SiMe_4$  as an external standard referenced to the solvents residual proton signal using the *xiref* AU program for  $^{13}C$  NMR spectra. DOSY NMR spectra were measured using the convection compensated

*dsteppgp3s* standard pulse sequence. Molar masses in solution were calculated using the Stalke-ECC-DOSY method (standard: adamantane or  $\text{Si}(\text{SiMe}_3)_4$ ).<sup>[50]</sup> ASAP-HSQC-spectra and ASAP-HSQC-DEPT-spectra were recorded using the published pulse sequences.<sup>[51]</sup> NOAH experiments were performed using the GENESIS tool<sup>[52]</sup> based on the published pulse programs.<sup>[53]</sup>

**General procedure of iGMM with amines:** Magnesium (10 mmol, 1 equiv.) and amine (10 mmol, 1 equiv.) were suspended in an ethereal solvent (10–20 mL, 0.5–1 M). EtBr (10 mmol, 1 equiv.) was added in 2–5 portions over 30 min at room temperature. The reaction mixture was stirred for one hour at room temperature. The conversion to the amide was determined by titration of a hydrolyzed aliquot with sulphuric acid (0.1 N) against phenolphthalein or by Gilman titration of an aliquot with benzoic acid against 4-phenyl-azo-diphenylamine. Typical yields are in the range of 40 to 95%.

**[(thf)<sub>3</sub>Mg(N(C<sub>6</sub>F<sub>5</sub>)<sub>2</sub>)<sub>2</sub>(Br)]:** Magnesium turnings (70 mg, 2.9 mmol, 1 equiv.) and  $\text{HN}(\text{C}_6\text{F}_5)_2$  (1 g, 2.9 mmol, 1 equiv.) were suspended in THF (3 mL) and EtBr (220  $\mu\text{L}$ , 2.9 mmol, 1 equiv.) was added in one portion. After 30 minutes an excess of EtBr (0.5 equiv.) was added, and the reaction mixture was stirred for 60 min at room temperature. The colorless solution was stored at 4 °C for 24 h, yielding the amide as colorless blocks. The crystals were collected by filtration and dried carefully *in vacuo*. Yield: 1.4 g, 2.4 mmol, 82%, <sup>1</sup>H NMR (400 MHz, [D<sub>8</sub>]THF, 297 K) = 3.64 (m, 12 H, thf), 1.80 (m, 12H, thf) ppm; <sup>13</sup>C NMR (101 MHz, [D<sub>8</sub>]THF, 297 K) = 141.5 (d, *J* = 233.6 Hz), 137.9 (d, *J* = 248.8 Hz), 132.3 (d, *J* = 239.3 Hz), 68.8, 26.7 ppm; <sup>19</sup>F NMR (376.5 MHz, [D<sub>8</sub>]THF, 297 K) = -159.2 (s, 2F, o), -169.0 (t, *J* = 21.5 Hz, 2F, m), -177.9 (1F, p) ppm, IR (ATR,  $n$  [cm<sup>-1</sup>]) = 2980 (w), 2892 (w), 1499 (vs), 1469 (s), 1191 (m), 1023 (vs), 1003 (vs), 878 (m).

**[(Et<sub>2</sub>O)<sub>6</sub>Mg<sub>6</sub>(N-*p*-Tol)<sub>4</sub>(Br)<sub>4</sub>]:** *p*-Toluidine (3.00 g, 28 mmol, 1 equiv.) and magnesium turnings (1.43 g, 59 mmol, 2.1 equiv.) were suspended in Et<sub>2</sub>O (30 mL) and EtBr (4.39 mL, 59 mmol, 2.1 equiv.) was added dropwise over 30 min. After addition of one eq. EtBr a colorless precipitate was observed, which redissolved completely after addition of the second eq. of EtBr. The reaction mixture was heated to reflux for two hours, 1,4-dioxane (2.5 mL, 1 equiv.) was added slowly at room temperature and the precipitate settled overnight at room temperature. The suspension was filtered (G3, diatomaceous earth), washed with Et<sub>2</sub>O and the volume of the filtrate was reduced to 1/5 under reduced pressure. Toluene (20 mL) was added and the colorless solution was stored at room temperature for 24 h. A few colorless crystals of [(Et<sub>2</sub>O)<sub>6</sub>MgBr<sub>2</sub>]<sub>2</sub> precipitated. The mother liquor was decanted, all solvents were removed *in vacuo* and the residue was redissolved in Et<sub>2</sub>O (20 mL). After storage for 24 h at room temperature the crystalline precipitate was collected and dried carefully under reduced pressure. [(Et<sub>2</sub>O)<sub>6</sub>Mg<sub>6</sub>(N-*p*-Tol)<sub>4</sub>(Br)<sub>4</sub>] (3.73 g, 4.18 mmol, 59%) was isolated as colorless blocks. <sup>1</sup>H NMR (400 MHz, [D<sub>8</sub>]-Tol, 297 K) = 1.00 (t, *J* = 6.9 Hz, 36H, Et<sub>2</sub>O), 2.31 (s, 12H, *p*-Tol), 3.71 (q, *J* = 6.9 Hz, 24H, Et<sub>2</sub>O), 6.88 (d, *J* = 8.3 Hz, 8H, *p*-Tol), 7.25 (d, *J* = 8.3 Hz, 8H, *p*-Tol) ppm, <sup>13</sup>C NMR (101 MHz, [D<sub>8</sub>]-Tol, 297 K) = 12.8, 20.4, 64.1, 120.5, 124.2, 128.8, 137.0, 161.2 ppm, <sup>15</sup>N NMR (40.6 MHz, [D<sub>8</sub>]-Tol, 297 K) = 108 ppm, IR (ATR,  $n$  [cm<sup>-1</sup>]) = 2970 (w), 2921 (w), 2864 (w), 1600 (m), 1507 (s), 1240 (s), 1222 (s), 1039 (m), 890 (m).

**[(thf)<sub>3</sub>Mg(3,6-Me<sub>2</sub>Carb)(Br)] (NMR scale):** 3,6-Dimethylcarbazole (30.1 mg, 154  $\mu\text{mol}$ , 1 equiv.) and magnesium (turnings, 7.5 mg, 308  $\mu\text{mol}$ , 2 equiv.) were suspended in [D<sub>8</sub>]THF (550.0  $\mu\text{L}$ ) and EtBr (11.4  $\mu\text{L}$ , 154  $\mu\text{mol}$ , 1 equiv.) was added in one portion. <sup>1</sup>H NMR (400 MHz, [D<sub>8</sub>]THF, 297 K):  $\delta$  = 7.72 (s, 2H, CzH), 7.52 (d, 2H, CzH), 6.98 (d, 2H, CzH), 2.45 (s, 6H, CH<sub>3</sub>), <sup>13</sup>C NMR: (100 MHz, [D<sub>8</sub>]THF, 297 K):  $\delta$  = 148.6 (CzC), 124.9 (CzC), 124.3 (CzC), 122.5 (CzC), 118.9 (CzC), 113.2 (CzC), 20.9 (CH<sub>3</sub>).

**[(Et<sub>2</sub>O)(Br)Mg- $\mu$ -(3,5-Me<sub>2</sub>pz)<sub>2</sub>-Mg(Br)(OEt<sub>2</sub>)]:** 3,5-Dimethylprazole (1.0 g, 10.4 mmol, 1 equiv.) and magnesium (turnings, 0.25 g, 10.4 mmol, 1 equiv.) were suspended in Et<sub>2</sub>O (10.5 mL) and EtBr (0.77 mL, 10.4 mmol, 1 equiv.) was added in three portions over 30 min. During the addition of EtBr a colorless amorphous solid began to precipitate. The reaction mixture was stirred overnight at room temperature. The solvent was removed under reduced pressure and the residue was dissolved in hot toluene (10 mL). Storage at -20 °C for 24 h yielded the pyrazolate as large colorless blocks. The precipitate was collected on a G2 frit and dried carefully under reduced pressure. Yield: 4.7 g, 8.4 mmol, 82%. Analytical data for [(Et<sub>2</sub>O)(Br)Mg- $\mu$ -(3,5-Me<sub>2</sub>pz)<sub>2</sub>-Mg(Br)(OEt<sub>2</sub>)] (major compound): <sup>1</sup>H NMR (400 MHz, C<sub>6</sub>D<sub>6</sub>, 297 K):  $\delta$  = 5.79 (s, 1H), 3.27 (q, *J* = 6.7 Hz, Et<sub>2</sub>O), 2.50 (s, 6H), 1.00 (t, *J* = 6.7 Hz, <sup>13</sup>C NMR (101 MHz, C<sub>6</sub>D<sub>6</sub>, 297 K):  $\delta$  = 151.7, 105.8, 65.5, 14.7, 13.4; Analytical data for [(Et<sub>2</sub>O)(Br)Mg- $\mu$ -(3,5-Me<sub>2</sub>pz)<sub>2</sub>- $\mu$ -Et<sub>2</sub>O-Mg(Br)(OEt<sub>2</sub>)] (minor compound): <sup>1</sup>H NMR (400 MHz, C<sub>6</sub>D<sub>6</sub>, 297 K):  $\delta$  = 5.68 (s, 1H), 3.27 (q, *J* = 6.7 Hz, Et<sub>2</sub>O), 2.29 (s, 3H), 2.17 (s, 3H), 1.00 (t, *J* = 6.7 Hz, <sup>13</sup>C NMR (101 MHz, C<sub>6</sub>D<sub>6</sub>, 297 K):  $\delta$  = 151.1, 105.5, 65.5, 14.7, 12.8.

**Crystal structure determinations:** The intensity data for the compounds were collected on a Nonius KappaCCD diffractometer using graphite-monochromated Mo-K $\alpha$  radiation. Data were corrected for Lorentz and polarization effects; absorption was taken into account on a semi-empirical basis using multiple-scans.<sup>[54–57]</sup> The structures were solved by intrinsic methods (SHELXT)<sup>[58]</sup> and refined by full-matrix least squares techniques against F<sub>o</sub><sup>2</sup> SHELXL-2018.<sup>[59]</sup> All hydrogen atoms were included at calculated positions with fixed thermal parameters. The crystals of [(thf)<sub>3</sub>Mg(NPh<sub>2</sub>)<sub>2</sub>], [(thf)<sub>3</sub>Mg<sub>2</sub>(Pz)<sub>2</sub>Br<sub>2</sub>], and [(Et<sub>2</sub>O)Mg]<sub>6</sub>(N-*p*-Tol)<sub>4</sub>( $\mu_3$ -Br)<sub>4</sub>] contained large voids, filled with disordered solvent molecules. The size of the voids was 1389, 580, and 385 Å<sup>3</sup>/unit cell, respectively. Their contribution to the structure factors was secured by back-Fourier transformation using the SQUEEZE routine of the program PLATON<sup>[60]</sup> resulting in 533, 156, and 86 electrons/unit cell, respectively. All non-hydrogen atoms were refined anisotropically.<sup>[58]</sup> Crystallographic data as well as structure solution and refinement details are summarized in Table S1. XP<sup>[61]</sup> was used for structure representations.

## Supporting Information

Deposition Number(s) 2169046 for [(thf)<sub>2</sub>Mg(NPh<sub>2</sub>)<sub>2</sub>], 2169047 for [(thf)<sub>3</sub>Mg(N(C<sub>6</sub>F<sub>5</sub>)<sub>2</sub>)<sub>2</sub>Br], 2169048 for [(thf)<sub>3</sub>Mg<sub>2</sub>(Pz)<sub>2</sub>Br<sub>2</sub>], 2169049 for [(Et<sub>2</sub>O)Mg(Pz)Br]<sub>2</sub>, 2169050 for [(Et<sub>2</sub>O)Mg]<sub>6</sub>(N-*p*-Tol)<sub>4</sub>( $\mu_3$ -Br)<sub>4</sub>, and 2169051 for [(Et<sub>2</sub>O)Mg]<sup>TBDM<sub>52</sub></sup>CpBr contain(s) the supplementary crystallographic data for this paper. These data are provided free of charge by the joint Cambridge Crystallographic Data Centre and Fachinformationszentrum Karlsruhe Access Structures service.

## Acknowledgements

We acknowledge the valuable support of the NMR service platform (www.nmr.uni-jena.de/) of the Faculty of Chemistry and Earth Sciences of the Friedrich Schiller University Jena, Germany. Parts of the equipment were provided by the German Research Foundation (DFG, INST 275/442-1 FUGG) which we kindly acknowledge. P. Schüler is very grateful to the German Environment Foundation (Deutsche Bundesstiftung Umwelt,

DBU, grant no. 20018/578) for a generous Ph.D. grant. Open Access funding enabled and organized by Projekt DEAL.

## Conflict of Interest

The authors declare no conflict of interest.

## Data Availability Statement

The data that support the findings of this study are available in the supplementary material of this article.

**Keywords:** amides · Grignard reaction · Hauser bases · magnesium · magnesocenes

- [1] M. Westerhausen, J. Langer, S. Krieck, C. Glock, *Rev. Inorg. Chem.* **2011**, *31*, 143–184.
- [2] a) F. Bickelhaupt, *Pure Appl. Chem.* **1986**, *58*, 537–542; b) F. Bickelhaupt, *Angew. Chem.* **1987**, *99*, 1020–1035; *Angew. Chem. Int. Ed. Engl.* **1987**, *26*, 990–1005; c) F. Bickelhaupt, *Pure Appl. Chem.* **1990**, *62*, 699–706; d) F. Bickelhaupt, *J. Organomet. Chem.* **1994**, *475*, 1–14; e) D. Seyferth, *Organometallics* **2009**, *28*, 1598–1605; f) R. M. Peltzer, J. Gauss, O. Eisenstein, M. Cascella, *J. Am. Chem. Soc.* **2020**, *142*, 2984–2994.
- [3] a) P. E. Eaton, C. H. Lee, Y. Xiong, *J. Am. Chem. Soc.* **1989**, *111*, 8016–8018; b) M. Shilai, Y. Kondo, T. Sakamoto, *J. Chem. Soc. Perkin Trans. 1* **2001**, 442–444.
- [4] L. Lochmann, *Eur. J. Inorg. Chem.* **2000**, 1115–1126.
- [5] a) R. E. Mulvey, *Chem. Commun.* **2001**, 1049–1056; b) R. E. Mulvey, *Organometallics* **2006**, *25*, 1060–1075; c) R. E. Mulvey, F. Mongin, M. Uchiyama, Y. Kondo, *Angew. Chem.* **2007**, *119*, 3876–3899; *Angew. Chem. Int. Ed.* **2007**, *46*, 3802–3824; d) R. E. Mulvey, *Acc. Chem. Res.* **2009**, *42*, 743–755; e) A. J. Martinez-Martinez, A. R. Kennedy, R. E. Mulvey, C. T. O'Hara, *Science* **2014**, *346*, 834–837; f) A. J. Martinez-Martinez, D. R. Armstrong, B. Conway, B. J. Fleming, J. Klett, A. R. Kennedy, R. E. Mulvey, S. D. Robertson, C. T. O'Hara, *Chem. Sci.* **2014**, *5*, 771–781; g) S. D. Robertson, M. Uzelac, R. E. Mulvey, *Chem. Rev.* **2019**, *119*, 8332–8405.
- [6] P. Caubière, *Chem. Rev.* **1993**, *93*, 2317–2334.
- [7] a) F. Blasberg, M. Bolte, M. Wagner, H.-W. Lerner, *Organometallics* **2012**, *31*, 1001–1005; b) T. Klatt, J. T. Markiewicz, C. Sämann, P. Knochel, *J. Org. Chem.* **2014**, *79*, 4253–4269; c) R. L.-Y. Bao, R. Zhao, L. Shi, *Chem. Commun.* **2015**, *51*, 6884–6900; d) D. S. Ziegler, B. Wei, P. Knochel, *Chem. Eur. J.* **2019**, *25*, 2695–2703.
- [8] a) B. Haag, M. Mosrin, H. Ila, V. Malakhov, P. Knochel, *Angew. Chem.* **2011**, *123*, 9968–9999; *Angew. Chem. Int. Ed.* **2011**, *50*, 9794–9824; b) A. D. Benischke, M. Ellwart, M. R. Becker, P. Knochel, *Synthesis* **2016**, 48, 1101–1107; c) A. J. Martinez-Martinez, C. T. O'Hara, *Adv. Organomet. Chem.* **2016**, *65*, 1–46; d) A. Kremsmair, J. H. Harenberg, K. Schwärzer, A. Hess, P. Knochel, *Chem. Sci.* **2021**, *12*, 6011–6019.
- [9] a) M. Westerhausen, M. Gärtner, R. Fischer, J. Langer, L. Yu, M. Reiher, *Chem. Eur. J.* **2007**, *13*, 6292–6306; b) M. Westerhausen, M. Gärtner, R. Fischer, J. Langer, *Angew. Chem.* **2007**, *119*, 1994–2001; *Angew. Chem. Int. Ed.* **2007**, *46*, 1950–1956; c) M. Westerhausen, J. Langer, S. Krieck, R. Fischer, H. Görls, M. Köhler, *Top. Organomet. Chem.* **2013**, *45*, 29–72; d) M. Westerhausen, A. Koch, H. Görls, S. Krieck, *Chem. Eur. J.* **2017**, *23*, 1456–1483.
- [10] a) C. R. Hauser, H. G. Walker, *J. Am. Chem. Soc.* **1947**, *69*, 295–297; b) F. C. Frostick, C. R. Hauser, *J. Am. Chem. Soc.* **1949**, *71*, 1350–1352; c) C. R. Hauser, C. R. Hance, *J. Am. Chem. Soc.* **1951**, *73*, 5846–5848.
- [11] a) R. Neufeld, D. Stalke, *Chem. Eur. J.* **2016**, *22*, 12624–12628; b) R. Neufeld, T. L. Teuteberg, R. Herbst-Irmer, R. A. Mata, D. Stalke, *J. Am. Chem. Soc.* **2016**, *138*, 4796–4806.
- [12] S. Krieck, P. Schüller, J. M. Peschel, M. Westerhausen, *Synthesis* **2019**, *51*, 1115–1122.
- [13] S. Dongmo, S. Zaubitzer, P. Schüller, S. Krieck, L. Jörissen, M. Wohlfahrt-Mehrens, M. Westerhausen, M. Marinaro, *ChemSusChem* **2020**, *13*, 3530–3538.
- [14] P. Schüller, S. Sengupta, S. Zaubitzer, F. Fiesinger, S. Dongmo, H. Görls, M. Wohlfahrt-Mehrens, M. van den Borg, D. Gaissmaier, S. Krieck, M. Marinaro, T. Jacob, M. Westerhausen, *Eur. J. Inorg. Chem.* **2022**, e202200149.
- [15] P. García-Álvarez, D. V. Graham, E. Hevia, A. R. Kennedy, J. Klett, R. E. Mulvey, C. T. O'Hara, S. Weatherstone, *Angew. Chem.* **2008**, *120*, 8199–8201; *Angew. Chem. Int. Ed.* **2008**, *47*, 8079–8081.
- [16] K.-C. Yang, C.-C. Chang, J.-Y. Huang, C.-C. Lin, G.-H. Lee, Y. Wang, M. Y. Chiang, *J. Organomet. Chem.* **2002**, *648*, 176–187.
- [17] M. L. Cole, P. C. Junk, *Z. Anorg. Allg. Chem.* **2015**, *641*, 2624–2629.
- [18] a) F. T. Edlmann, *Adv. Organomet. Chem.* **2008**, *57*, 183–352; b) C. Jones, *Coord. Chem. Rev.* **2010**, *254*, 1273–1289; c) A. Stasch, C. Jones, *Dalton Trans.* **2011**, *40*, 5659–5672; d) T. Chlupatý, A. Růžička, *Coord. Chem. Rev.* **2016**, *314*, 103–113.
- [19] P. C. Andrews, M. Bryn, C. Jones, P. C. Junk, M. Kloth, *Inorg. Chim. Acta* **2006**, *359*, 355–363.
- [20] a) J. Langer, S. Krieck, R. Fischer, H. Görls, D. Walther, M. Westerhausen, *Organometallics* **2009**, *28*, 5814–5820; b) R. Fischer, H. Görls, P. R. Meisinger, R. Suxdorf, M. Westerhausen, *Chem. Eur. J.* **2019**, *25*, 12830–12841.
- [21] T. Hascall, M. M. Olmstead, P. P. Power, *Angew. Chem.* **1994**, *106*, 1056–1057; *Angew. Chem. Int. Ed. Engl.* **1994**, *33*, 1000–1001.
- [22] a) P. Jutzi, *Adv. Organomet. Chem.* **1986**, *26*, 217–295; b) P. Jutzi, *J. Organomet. Chem.* **1990**, *400*, 1–17; c) T. P. Hanusa, *Chem. Rev.* **1993**, *93*, 1023–1036; d) D. J. Burkey, T. P. Hanusa, *Comments Inorg. Chem.* **1995**, *17*, 41–77; e) A. J. Bridgeman, *J. Chem. Soc. Dalton Trans.* **1997**, 2887–2893; f) P. Jutzi, N. Burford in *Metalloenes: Synthesis, Reactivity, Applications, Vol. 1* (Eds.: A. Togni, R. L. Halterman), Wiley-VCH, Weinheim, **1998**, pp. 3–54; g) N. J. Long, *Metalloenes: An Introduction to Sandwich Complexes*, Blackwell Science, Oxford, **1998**; h) P. Jutzi, N. Burford, *Chem. Rev.* **1999**, *99*, 969–990; i) P. Jutzi, G. Reumann, *J. Chem. Soc. Dalton Trans.* **2000**, 2237–2244; j) T. P. Hanusa, *Organometallics* **2002**, *21*, 2559–2571; k) P. H. M. Budzelaar, J. J. Engelberts, J. H. van Lenthe, *Organometallics* **2003**, *22*, 1562–1576.
- [23] M. Westerhausen, N. Makropoulos, B. Wieneke, K. Karaghiosoff, H. Nöth, H. Schwenk-Kircher, J. Knizek, T. Seifert, *Eur. J. Inorg. Chem.* **1998**, 965–971.
- [24] C. P. Morley, P. Jutzi, C. Krüger, J. M. Wallis, *Organometallics* **1987**, *6*, 1084–1090.
- [25] M. Huber, H. Schnöckel, *Inorg. Chim. Acta* **2008**, *361*, 457–461.
- [26] T. Duan, H. Schnöckel, private CSD communication REVNOW, **2005**.
- [27] T. Duan, H. Schnöckel, private CSD communication REVNIQ, **2005**.
- [28] C. Dohmeier, D. Loos, C. Robl, H. Schnöckel, D. Fenske, *J. Organomet. Chem.* **1993**, *448*, 5–8.
- [29] P. Schüller, H. Görls, S. Krieck, M. Westerhausen, *Chem. Eur. J.* **2021**, *27*, 15508–15515.
- [30] a) S. Harder, *Chem. Commun.* **2012**, *48*, 11165–11177; b) M. M. D. Roy, A. A. Omana, A. S. S. Wilson, M. S. Hill, S. Aldrige, E. Rivard, *Chem. Rev.* **2021**, *121*, 20, 12784–12965. See also: C. Bakewell, *Dalton Trans.* **2020**, *49*, 11354–11360.
- [31] a) H. M. Walborsky, *Acc. Chem. Res.* **1990**, *23*, 286–293; b) J. F. Garst, *Acc. Chem. Res.* **1991**, *24*, 95–97; c) C. Hamdouchi, M. Topolski, V. Goedken, H. M. Walborsky, *J. Org. Chem.* **1993**, *58*, 3148–3155; d) J. F. Garst, M. P. Soriaga, *Coord. Chem. Rev.* **2004**, *248*, 623–652.
- [32] M. Gärtner, R. Fischer, J. Langer, H. Görls, D. Walther, M. Westerhausen, *Inorg. Chem.* **2007**, *46*, 5118–5124.
- [33] A. Xia, M. J. Heeg, C. H. Winter, *Organometallics* **2002**, *21*, 4718–4725.
- [34] C. A. Fischer, A. Rösch, H. Elsen, G. Ballmann, M. Wiesinger, J. Langer, C. Färber, S. Harder, *Dalton Trans.* **2019**, *48*, 6757–6766.
- [35] C. J. Snyder, M. J. Heeg, C. H. Winter, *Inorg. Chem.* **2011**, *50*, 9210–9212.
- [36] D. Pfeiffer, M. J. Heeg, C. H. Winter, *Angew. Chem.* **1998**, *110*, 2674–2676; *Angew. Chem. Int. Ed.* **1998**, *37*, 2517–2519.
- [37] N. C. Mösch-Zanetti, M. Ferbinteanu, J. Magull, *Eur. J. Inorg. Chem.* **2002**, 950–956.
- [38] T. Kloubert, C. Müller, S. Krieck, T. Schotthauer, H. Görls, M. Westerhausen, *Eur. J. Inorg. Chem.* **2012**, 5991–6001.
- [39] T. Hascall, K. Ruhlandt-Senge, P. P. Power, *Angew. Chem.* **1994**, *106*, 350–351; *Angew. Chem. Int. Ed. Engl.* **1994**, *33*, 356–357.
- [40] W. J. Grigsby, T. Hascall, J. J. Ellison, M. M. Olmstead, P. P. Power, *Inorg. Chem.* **1996**, *35*, 3254–3261.
- [41] B. M. Wolf, R. Anwänder, *Chem. Eur. J.* **2019**, *25*, 8190–8202.
- [42] C. N. de Bruin-Dickason, G. B. Deacon, C. Jones, P. C. Junk, M. Wiecko, *Eur. J. Inorg. Chem.* **2019**, 1030–1038.



- [43] a) D. Tan, F. Garcia, *Chem. Soc. Rev.* **2019**, *48*, 2274–2292; b) D. Jedrzkiewicz, J. Langer, S. Harder, *Z. Anorg. Allg. Chem.* **2022**, e202200138.
- [44] N. C. Boyde, N. R. Rightmire, T. P. Hanusa, W. W. Brennessel, *Inorganics* **2017**, *5*, 36.
- [45] R. F. Koby, A. M. Doerr, N. R. Rightmire, N. D. Schley, B. K. Long, T. P. Hanusa, *Angew. Chem.* **2020**, *132*, 9629–9635; *Angew. Chem. Int. Ed.* **2020**, *59*, 9542–9548.
- [46] M. Berton, K. Sheehan, A. Adamo, D. T. McQuade, *Beilstein J. Org. Chem.* **2020**, *16*, 1343–1356.
- [47] H. Matsubara, Y. Niwa, R. Mataka, *Synlett* **2015**, *26*, 1276–1280.
- [48] B. A. Dalvi, P. D. Lokhande, *Tetrahedron Lett.* **2018**, *59*, 2145–2149.
- [49] R. Koppang, *Acta Chem. Scand.* **1971**, *25*, 3067–3071.
- [50] R. Neufeld, D. Stalke, *Chem. Sci.* **2015**, *6*, 3354–3364.
- [51] a) D. Schulze-Sünnighausen, J. Becker, B. Luy, *J. Am. Chem. Soc.* **2014**, *136*, 1242–1245; b) D. Schulze-Sünnighausen, J. Becker, M. R. M. Koos, B. Luy, *J. Magn. Reson.* **2017**, *281*, 151–161.
- [52] J. R. J. Yong, Ě. Kupče, T. D. W. Claridge, *Anal. Chem.* **2022**, *94*, 2271–2278.
- [53] a) Ě. Kupče, T. D. W. Claridge, *Angew. Chem.* **2017**, *129*, 11941–11945; *Angew. Chem. Int. Ed.* **2017**, *56*, 11779–11783; b) J. R. J. Yong, A. L. Hansen, Ě. Kupče, T. D. W. Claridge, *J. Magn. Reson.* **2021**, *329*, 107027.
- [54] R. Hooft: COLLECT, Data Collection Software; Nonius B. V., Netherlands, **1998**.
- [55] Z. Otwinowski, W. Minor, in *Methods in Enzymology* (Eds. C. W. Carter, R. M. Sweet), vol. 276, part A, Academic Press, San Diego, USA, **1997**, pp. 307–326.
- [56] a) SADABS 2.10, Bruker-AXS Inc., **2002**, Madison, WI, USA; b) SADABS 2016/2: L. Krause, R. Herbst-Irmer, G. M. Sheldrick, D. Stalke, *J. Appl. Crystallogr.* **2015**, *48*, 3–10.
- [57] Bruker (2020) APEX3 Bruker AXS LLC, Madison, WI, USA.
- [58] G. M. Sheldrick, *Acta Crystallogr. Sect. A* **2015**, *71*, 3–8.
- [59] G. M. Sheldrick, *Acta Crystallogr. Sect. C* **2015**, *71*, 3–8.
- [60] A. L. Spek, *Acta Crystallogr. Sect. C* **2015**, *71*, 9–18.
- [61] XP, Siemens Analytical X-ray Instruments Inc., Karlsruhe, Germany, **1990**; Madison, WI, USA, **1994**.

---

Manuscript received: May 3, 2022

Accepted manuscript online: June 10, 2022

Version of record online: July 19, 2022